Reactive Power Impacts on LCL Filter Capacitor Lifetime in Grid-Connected Inverter

DAO ZHOU (Senior Member, IEEE), HUAI WANG (Senior Member, IEEE), AND FREDE BLAABJERG (Fellow, IEEE)

Department of Energy Technology, Aalborg University 9100, Aalborg, Denmark

CORRESPONDING AUTHOR: DAO ZHOU (e-mail: zda@et.aau.dk)

ABSTRACT With the increasing penetration of renewable power, its reliability and cost-effective production are becoming more important. A filter is inserted between the grid-connected inverter and the power grid to reduce the PWM switching harmonics, which may become a fragile part seen from the power electronics converter perspective. As the grid-connected inverter is typically designed with additional reactive power capability, this paper tries to investigate the additional stresses of the filter capacitor introduced by the reactive power injection. According to an electro-thermal stress evaluation, the time-to-failure distribution of a single LCL filter capacitor is investigated in detail. Moreover, the increasing equivalent series resistance along with the operational period is taken into account. Aiming towards a system-level reliability analysis, a Weibull distribution based reliability of an individual capacitor can be linked to the reliability of a capacitor bank by using a reliability block diagram. A case study of a 2 MW wind power converter shows that the lifetime is significantly reduced from the individual capacitor to the capacitor bank. Besides, over-excited reactive power injection further reduces the lifetime of the LCL filter capacitors.

INDEX TERMS Power capacitors, lifetime estimation, reactive power, degradation.

I. INTRODUCTION

With the increased adoption of renewable energy for the power generation, the three-phase voltage source inverter has become an important interface to convert clean energy to the utility grid [1]. A filter is usually required in between to introduce a current feedback control. A single inductor filter can be used, but the harmonic attenuation may not be sufficient. Besides, a high voltage drop can be produced due to the bulky inductor. Especially in the high-power application, where the switching frequency is normally limited by the associated switching losses, such a simple configuration may lead to a costly passive filter and slow down the system dynamic response [2], [3]. Commonly, a high-order LCL filter is applied, as it achieves a higher attenuation along with the weight saving of the components. Compared with the single inductor filter, a smaller inductor and capacitor minimize the amount of current harmonics injection into the utility grid, which complies with the harmonic standards.

Due to the higher penetration of wind power integrated into the power grid, some utilities have launched more stringent operational regimes that establish similar requirements from conventional generating plants to wind power converters [4]. It indicates that the network supporting is mandatory. Additional reactive power is required to regulate the voltage level back to normal. As the wind turbines are usually located in remote areas, the unstable terminal voltage also asks for the reactive power to maintain a constant level [5].

The performance of power capacitor is complicated and highly affected by its operation conditions such as the voltage, current, frequency, and temperature. Many researchers have investigated the degradation of electrolytic capacitors [6]–[10]. For instance, a real-time failure detection method is developed for the changes of the equivalent series resistance (ESR) and the capacitance of the capacitors [7]. Lifetime prediction models of electrolytic capacitors are established for switch-mode power supplies and variable-frequency

drives [8], [9]. These electrolytic capacitors commonly form passive DC-links, which are one of the highest failure rate components and contribute to more than 20% of failure in certain applications [11]. However, few studies investigate the degradation effect on reliable operation of the film capacitor, which is the key candidate for the LCL filter capacitor banks. Since the filter capacitor is directly linked to the power grid, the voltage swell and dip, unbalanced voltage, background harmonic may have a great impact on the capacitor electro-thermal stresses. High ripple currents cause internal self-heating and hot-spot temperature, which results in aging. Moreover, it can increase capacitor ESR over time, which causes more heating for a given ripple current, thus increasing the core temperature and accelerating the degradation process [11]. There are plenty of field examples of filter capacitor banks failures [12], but the analytical relationship between the grid condition and degradation of the filter capacitor is not clear. This paper develops an approach to evaluate the reliability of the film capacitor used in an LCL filter. Moreover, the influence of the reactive power is taken into account, along with the produced real power from the wind conditions. It is a physics-of-failure approach from the component-level [13]–[16] to system-level reliability, which considers the parameter shifts of ESR and capacitance due to degradation.

The remaining parts of the paper are organized as follows. Section II describes the failure mechanism of the LCL filter capacitor. The reactive power impacts on the capacitor electrical stresses are analyzed in Section III. Afterwards, Section IV investigates and compares the time-to-failure from a capacitor cell to the capacitor bank. Finally, concluding remarks are drawn in the last section.

II. FAILURE MODES OF LCL FILTER CAPACITOR

As shown in Fig. 1(a), due to lots of switching harmonic voltage introduced by the Pulse Width Modulation (PWM) inverter, a filter is normally applied to mitigate the corresponding harmonic current flowing into the grid [17]. Since the renewable power generation systems are typically installed in remote areas, the PWM inverter is required to potentially provide or absorb the reactive power to support the grid voltage regulation. The reactive power profile specified in the German grid codes is shown in Fig. 1(b) [18], in which NOR represents the normal operation (i.e., the reactive power is zero). It is noted that different amounts of the Over-Excited (OE) and Under-Excited (UE) reactive power are required along with the various active power production.

Seen from the power grid, as the LCL filter features a lower impedance at the switching-frequency compared to the single inductor filter, it is generally a preferred solution in the grid-connected inverter. The design procedure of the LCL filter is well described in [19], [20], where the filter capacitor is designed with the additional introduced reactive power.

It is well known that various types of power capacitors are used in inverters. Electrolytic capacitors are applied in the case of high capacitance per volume (e.g., DC-link applications). Wear-out failure mechanisms in electrolytic capacitors
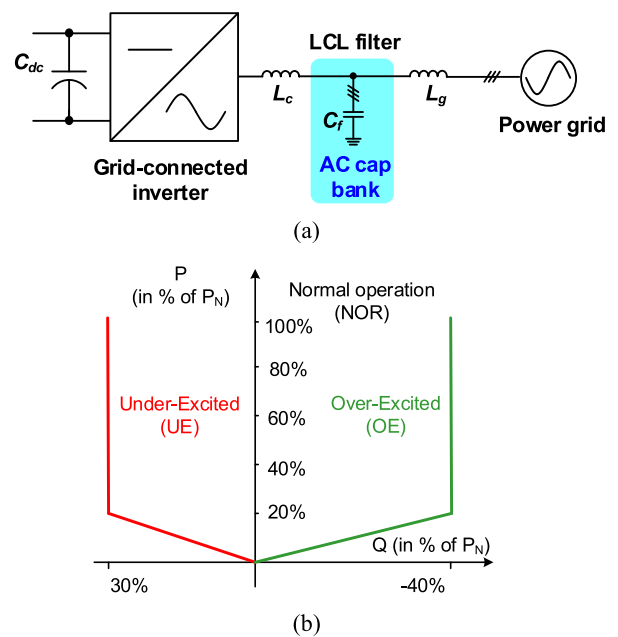

FIGURE 1. **Grid-connected inverter with filter capacitive bank (AC cap bank).(a) Configuration; (b) Reactive power requirement from German grid codes.**

are usually caused by the chemical effect in the dielectric, which is closely related to the temperature, and voltage level. Due to the electrolyte loss, the time-temperature chemical degradation process doubles for each 10 °C rise in temperature [21]. Time-voltage degradation caused by the electrochemical reaction is more difficult to quantify, because it is dependent on the dielectric type. Due to the low withstand voltage and the unchangeable polarity of the electrolytic capacitor, the metalized film capacitors are more preferable in the grid filter due to the high electric-field stress. Moreover, the material of polypropylene (PP) is preferred compared to polyethylene terephthalate (PET) because of a much lower loss factor [11]. One of the main failure mechanisms of film capacitors is related to thermal stress induced by ambient temperature and internal temperature rise due to ripple current and leakage current. The leakage current becomes higher with higher voltage stress and temperature stress.

III. REACTIVE POWER IMPACT ON ELECTRICAL STRESSES OF CAPACITOR

Based on the modulation scheme of the power converter, this section starts with electrical stresses analysis (e.g., the flowing current, and across voltage) of the filter capacitor with the help of the LCL filter impedance characteristics. In the case of wind power generation, the loading condition and reactive current impact on electrical stresses of the filter capacitor are investigated.

A. ELECTRICAL STRESSES OF FILTER CAPACITOR

To fully utilize the DC-link voltage, the Space Vector Modulation (SVM) is usually applied in the three-phase system. As
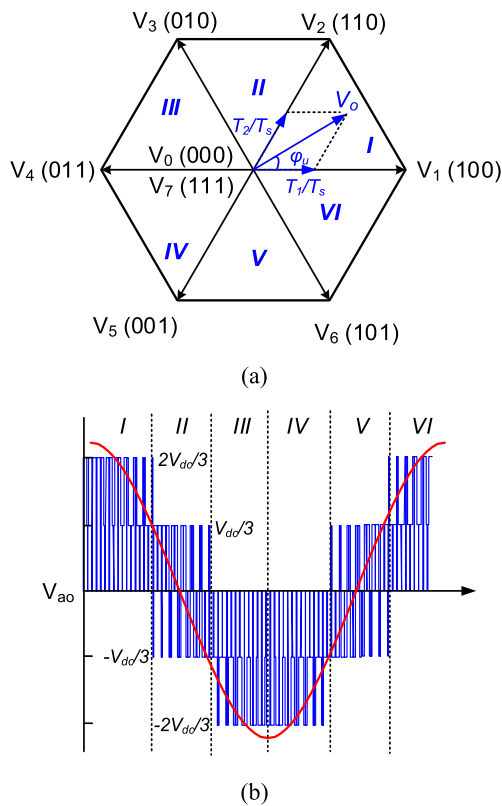
TABLE 1. Parameters of 2 MW DFIG System

Rated power	2 MW
Rated amplitude of phase voltage	563 V
Grid-side inductor	125 µH
Converter-side inductor	125 µH
Filter capacitor	300 µF
DC-link voltage	1050 V
Switching frequency	2 kHz

FIGURE 2. Illustration of space vector modulation. (a) Six sectors. (b) Phase voltage of converter output within a fundamental period.

FIGURE 3. LCL filter characteristic from converter voltage to filter capacitor voltage and current.

shown in Fig. 2(a), six sectors (Sector I to VI) can be divided in accordance with the phase angle of the output voltage φ_u. In the case of the Sector I, depending on various switching states of the power devices, it can be seen that the inverter output voltage V_o includes the levels of $2V_{dc}/3$, $V_{dc}/3$, and 0, where V_{dc} is the DC-link voltage. By using a similar approach, the voltage waveform of the inverter output can be expected in the other five sectors, which is consistent with three voltage levels within the same sector as described in Fig. 2(b).

For the LCL filter, the majority of the harmonic current goes through the capacitor branch, while the fundamental current flows into the power grid to achieve high power quality. In order to calculate the harmonic components of the filter capacitor current and voltage, it is necessary to perform a Fourier analysis, which starts with the analysis of the converter voltage. For a pulsed voltage, the Fourier coefficients can be calculated by its starting and ending time instants together with its voltage amplitude. With the information of voltage amplitude in various sectors, the Fourier coefficients can further be accumulated from a single switching period to the entire fundamental period [15], [22]. Thereafter, the harmonic components of the converter voltage can be deduced.

The relationship between the converter voltage and filter capacitor electrical stresses is tightly dependent on the characteristics of the LCL filter. Although grid-tied applications cover a wide range like wind/photovoltaic generation, and energy storage system, etc., the control scheme and modulation

strategy for these applications are almost the same. For simplicity, the wind power generation is selected as a case study. With the parameters of the LCL filter of a 2 MW Doubly-Fed Induction Generator (DFIG) based wind turbine system listed in Table 1, the transfer functions from the converter voltage to the capacitor current and voltage are shown in Fig. 3.

Since the impedance of the filter capacitor C_f is significantly higher than the grid-side inductor L_g at the fundamental frequency, the fundamental component of the converter current i_{g1} directly flows into the power grid, and the harmonic components go through the filter capacitor. Consequently, under the fundamental frequency, the filter capacitor can be considered as open-circuit as shown in Fig. 4(a). In the case of the super-synchronous operation, the d-axis component of the grid current i_{gd1} becomes negative in order to provide the slip power from the induction generator into the power grid. Nevertheless, as shown in Fig. 4(b) and (c), the OE and UE reactive power injection makes the q-axis component of the grid current i_{gq1} positive and negative, respectively. As the voltage drop across the filter inductor u_{L1} leads the converter current 90°, its q-axis component u_{Ld1} is orthogonal to the grid voltage u_g, while its q-axis component u_{Ld1} is in the same or opposite direction with the grid voltage. It can be expected that the current reference at the q-axis has a higher impact on the amplitude of the converter voltage. Since the voltage drop across the converter-side inductor and the grid-side inductor is proportional to their inductance, the capacitor voltage can thereby be estimated. It is evident that the OE reactive
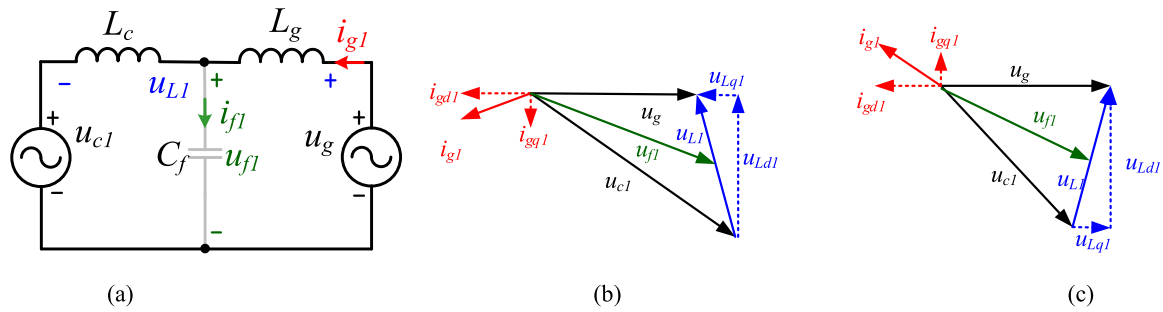
FIGURE 4. Relationship between the converter voltage and the filter capacitor electrical stresses in the case of the fundamental frequency. (a) Configuration of the LCL filter. (b) Vector diagram in the case of over-excited reactive power injection. (c) Vector diagram in the case of under-excited reactive power injection.
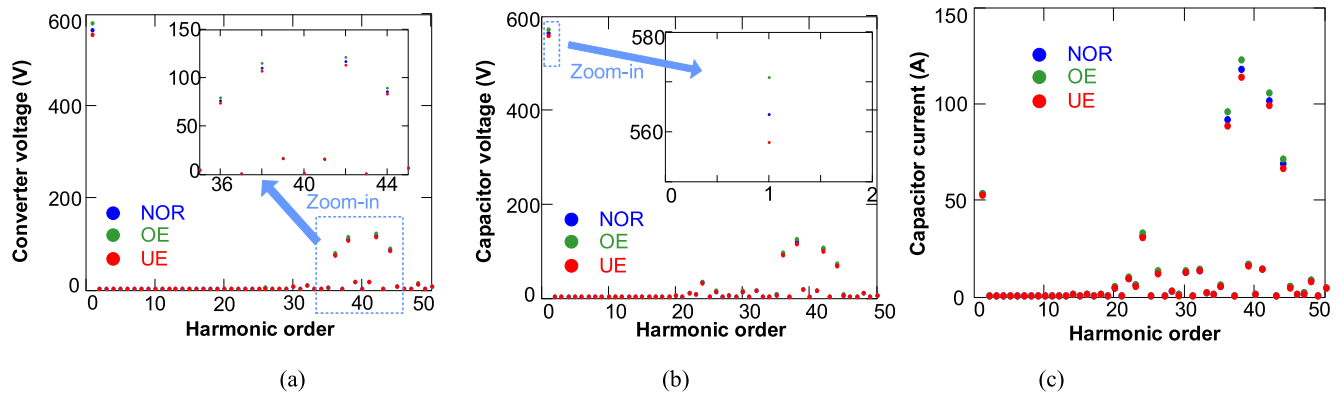

FIGURE 5. Reactive power effects on harmonic spectrum of filter capacitor voltage and current at rated wind speed. (a) Converter voltage. (b) Capacitor voltage. (c) Capacitor current. (NOR: normal operation; OE: over-excited reactive power injection; UE: under-excited reactive power injection).

power injection keeps the capacitor voltage higher than the grid voltage, while the UE reactive power injection makes the capacitor voltage lower than the power grid.

At the rated condition of the DFIG system, the harmonic spectrum of the capacitor voltage and current are calculated in Fig. 5. To analyze the converter voltage, the Fourier coefficient is accumulated from a single pulse to the whole fundamental period. It can be seen that, apart from the required fundamental voltage produced by the controlled grid current, the harmonic components of the converter voltage is dominant by the harmonic orders around the switching frequency. Then, the voltage and current harmonic spectrum of the filter capacitor can be investigated based on the aforementioned transfer function in Fig. 3. In the case of the NOR condition, it can be seen that the fundamental component of the capacitor voltage is similar to the grid voltage, due to the negligible orthogonal voltage drop across the filter capacitor compared to the grid voltage. In the case of reactive power operation, it is noted that the fundamental component of the capacitor voltage increases under the OE reactive power but decreases under the UE reactive power. Moreover, the OE reactive power injection increases the harmonic components of the capacitor voltage, while the UE reactive power injection decreases the harmonic components. In general, the fundamental component is significantly higher than the harmonic components in the converter and capacitor voltage. Nevertheless, as shown in Fig. 5(c), it can be seen that the capacitor current is around 50 A, which

fulfills the design criteria of the filter capacitor so that the capacitor current is around 10% of the rated current [19]. Although the fundamental component is comparable with the harmonic components, the capacitor current is still dominant by the harmonic components. In addition, it is evident that harmonic around 23rd order is amplified due to the resonant frequency of the LCL filter.

According to the relationship between the wind speed and generator output power [23], together with the reactive power profile as shown in Fig. 1(b), the electrical stresses of the filter capacitor can be calculated from the cut-in wind speed of 4 m/s to the rated wind speed of 12 m/s. As the fundamental component dominates the capacitor voltage, while the harmonic components determine the capacitor current, both of them are in focus as shown in Fig. 6. It can be seen that the OE reactive power increases the current and voltage stresses, while the UE reactive power relieves the electrical stresses throughout the whole operation conditions.

B. SIMULATION VALIDATION

In order to verify the aforementioned analytical approach for the LCL filter capacitor electrical stresses, the capacitor voltage and current are investigated in the simulation with focus on reactive power and loading impacts. The control strategy of 2 MW DFIG back-to-back power converter is the conventional vector control applied under the rotating reference frame [16].
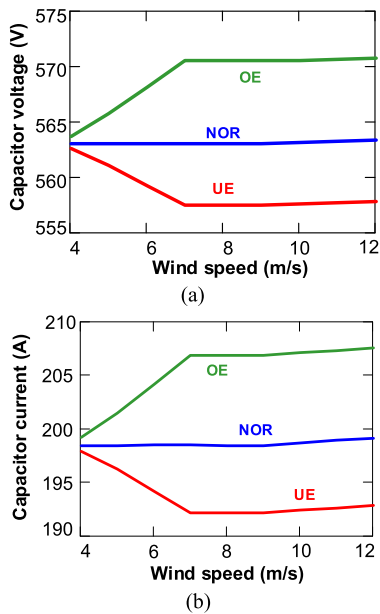
FIGURE 6. Electrical stresses of LCL filter capacitor with various wind speeds. (a) Fundamental component of capacitor voltage. (b) Harmonic components of capacitor current. (NOR: normal operation; OE: over-excited reactive power injection; UE: under-excited reactive power injection).

In the case of the rated power without reactive power injection, the simulated converter voltage, capacitor voltage, and capacitor current are shown in Fig. 7. Both the fundamental and harmonic components of the converter voltage totally agree with the theoretical analysis, where the harmonic components are mostly dominated by sidebands of the PWM switching. Apart from the fundamental and PWM switching harmonic components in the capacitor voltage, the harmonic components around 23rd order can be seen due to the resonant frequency of the LCL filter. Moreover, it can be seen that the fundamental component is much higher than the PWM switching harmonic. Nevertheless, the switching harmonics of the capacitor current are more important.

The reactive power and loading impacts on the electrical stresses of the capacitor are shown in the Fig. 8(a) and (b), respectively. Regardless of the reactive power direction, it can be seen that the fundamental component dominates the capacitor voltage, while the harmonic components determine the capacitor current. In addition, it is clear that the fundamental component of the capacitor voltage slightly increases in the case of the OE reactive power, while it decreases a little in the case of the UE reactive power. Besides, the loading impacts on the electrical stresses are evaluated in the case of the unity power factor. As shown in Fig. 8(b), it can be found that both the voltage and current of the capacitor are almost the same.

IV. TIME-TO-FAILURE AND RELIABILITY OF FILTER CAPACITOR BANK

Section III addresses the electrical stresses (flowing current and across voltage) of the filter capacitor at a certain wind speed. With an annual mission profile, the temperature and

voltage profiles of a single capacitor can be calculated according to capacitor electrical and thermal models. Together with the strength/lifetime modeling, where the accelerated lifetime testing results are sorted by Weibull distribution, the lifetime of the individual capacitor can thus be predicted. As the capacitor bank is configured with a set of capacitors, its system-level reliability can be investigated by using the reliability block diagram. Meanwhile, the parameter shifting of the ESR due to the degradation can be taken into account along with the operational period.

As aforementioned, the current and voltage stresses of the filter capacitor can be calculated at a certain wind speed. It can be found that the current stress is dominated by fundamental component and switching harmonics, while the voltage stress relies only on the fundamental component.

In respect to the power dissipation of filter capacitor, it can be expressed as,

$$P_{\text{loss}} = I_{f(1)}{}^2 \cdot ESR_{(1)} + \sum I_{f(sw)}{}^2 \cdot ESR_{(sw)} \qquad (1)$$

It is noted that the capacitor current I_f is divided into fundamental order (represented by subscript 1) and switching orders (represented by subscript sw), as the ESR of the capacitor is frequency dependent [26].

Afterwards, the core temperature of the capacitor T_x is jointly decided by the ambient temperature T_a and internal temperature rise caused by the loss dissipation,

$$T_x = P_{\text{loss}} \cdot R_{th} + T_a \qquad (2)$$

where R_{th} denotes the capacitor thermal resistance from the core to the ambient.

By knowing the applied voltage V_x and core temperature T_x, the stress analysis of the filter capacitor is readily acquired. Afterwards, an accelerated lifetime testing is usually performed to obtain the strength modeling. An example of electrolytic capacitor has been presented in [28]. A series of 9 capacitors are tested at the rated voltage, rated ripple current, and upper operational temperature [24]. The normalized capacitance and ESR are regularly measured until the component is worn-out completely. Although the same standard (20% of capacitance drop) is considered as the end-of-life criteria, the testing hours to failure for each component varies due to the parameter deviation and tolerance. To sort the lifetime data with a reasonable confidence level, the Weibull distribution is widely used in the reliability engineering [11], [13].

The probability density function of Weibull function $f(t)$ is known as,

$$f(t) = \frac{\beta}{\eta} \cdot \left(\frac{t}{\eta}\right)^{\beta-1} \cdot \exp\left[-\left(\frac{t}{\eta}\right)^{\beta}\right] \qquad (3)$$

Since the unreliability/failure function $F(t)$ is defined as the integral of the probability density function, the cumulative density function can be deduced as,

$$F(t) = 1 - \exp\left[-\left(\frac{t}{\eta}\right)^{\beta}\right] \qquad (4)$$
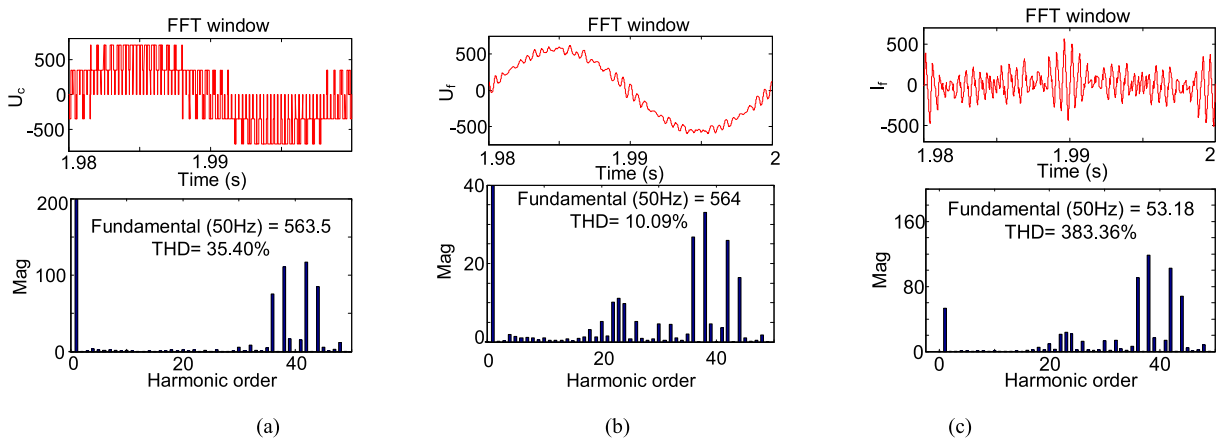
FIGURE 7. Harmonic spectrum of filter voltage and current at rated wind speed operation at unity power factor. (a) Converter voltage. (b) Capacitor voltage. (c) Capacitor current.
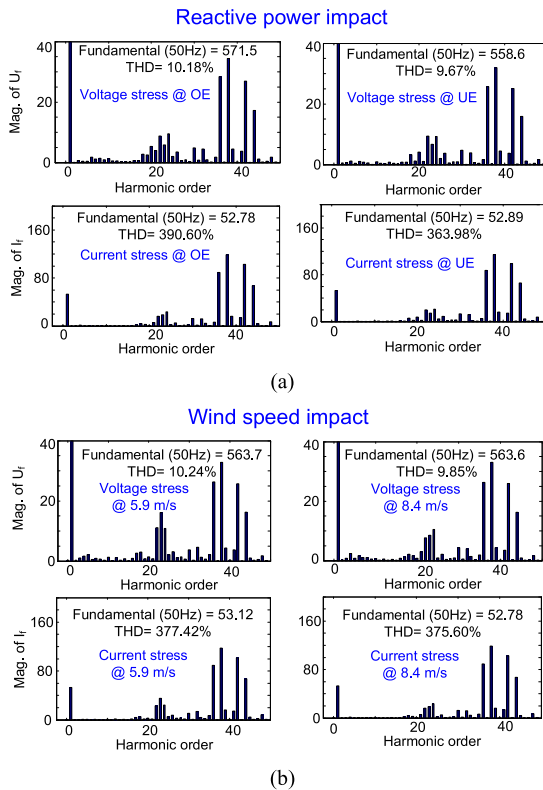

FIGURE 8. Harmonic spectrum of capacitor voltage and current at various operation modes. (a) Impacts of reactive power at the rated wind speed. (b) Impacts of wind speeds with unity power factor. (OE: over-excited reactive power injection; UE: under-excited reactive power injection).

where β denotes the shape factor, while η denotes the scale factor. Based on the value of the shape parameter, it is a versatile distribution that can represent the characteristics of other types of distributions (e.g., Exponential distribution) [27].

With the help of raw data from the accelerated test, these points can be reflected in unreliability plot with the confirmed sample size [27]. The scale parameter and shape parameter

of the Weibull distribution can thus be deduced by using curve fitting. Then, the B_x lifetime can be complied from the unreliability plot. The same testing procedure can propagate to other lower stress conditions within a reasonable testing period. Consequently, similar results can be obtained with lower applied voltage and core temperature.

For the 2 MW wind turbine, the equivalent 100 μF filter capacitor is applied, which in practice is realized by 10 pieces of 10 μF/780V from a leading capacitor manufacturer [25]. Compared with the filter capacitor used in the field, the general procedure to obtain the lifetime model can be considered to be the same.

As the film capacitor is sensitive to the applied voltage (following the power law) and the core temperature (following the Arrhenius law), the lifetime model of the capacitor can be expressed as [26],

$$L_x = L_r \cdot 2^{\frac{T_r - T_x}{n_1}} \cdot \left(\frac{V_r}{V_x}\right)^{n_2} \tag{5}$$

where L_x denotes the hours to failure used in the real application, while L_r denotes the hours to the failure at the rated voltage V_r, and upper categorized temperature T_r. n_1 denotes acceleration coefficient due to the core temperature T_x. Another factor lies in the applied voltage V_x with the exponent coefficient n_2.

With the aid of the stress analysis (applied voltage V_x and core temperature T_x) and the strength model (temperature factor n_1 and voltage factor n_2) of the capacitor, the lifecycle of the single capacitor L_x can be calculated at a certain wind speed based on (5). Moreover, the degrading ESR from the accelerated tests can be considered in the loss model.

Afterwards, its B_{10} lifetime L_{B10_com} can be predicted by considering the whole annual wind profile. With the shape factor of the Weibull distribution from the degradation test, its percentile B_{10} lifetime of the individual capacitor can be further translated into the time-dependent unreliability curve F_{com}. Considering the configuration and structure of the whole capacitor bank, its system-level unreliability curve F_{sys} can be
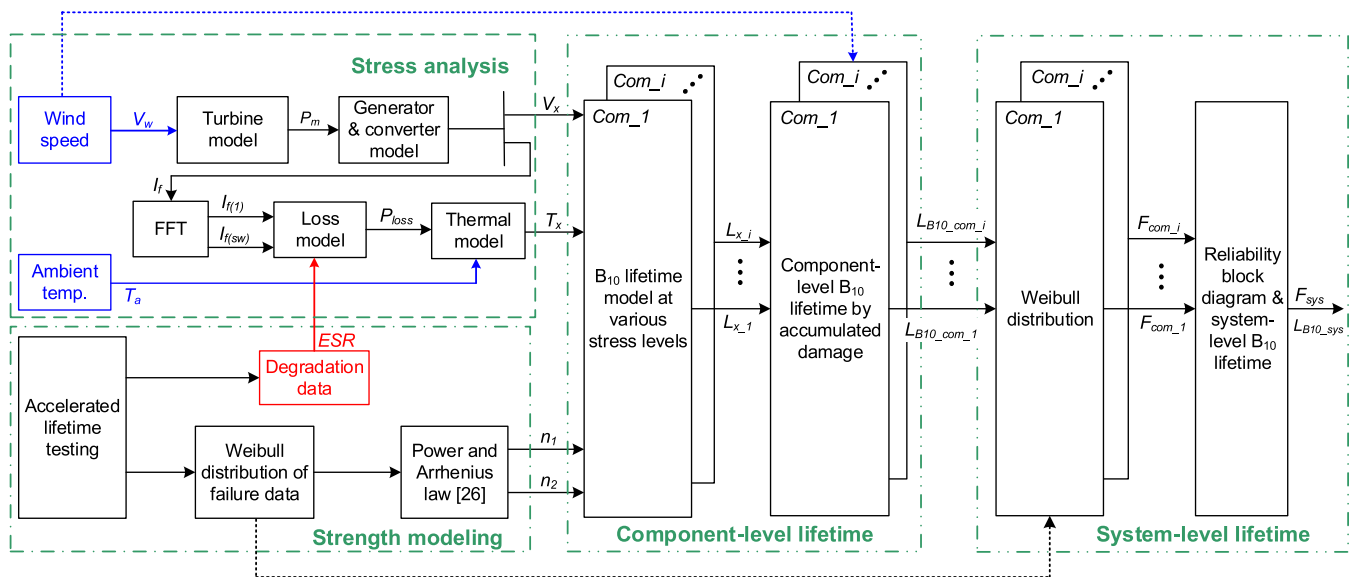
FIGURE 9. Reliability evaluation flowchart from mission profile to component-level and system-level capacitor lifetime.

TABLE 2. Key Parameters Related to Core Temperature and Lifetime of Capacitor

Core temperature	ESR	3 mΩ @10 kHz
	Thermal resistance from core to ambient	14.1 °C/W
Lifetime	Rated hours to failure L_r	100,000
	Rated temperature T_r	75 °C
	Temperature coefficient n_1	10
	Rated voltage V_r	780 V
	Voltage coefficient n_2	0.7

calculated from component-level unreliability F_{com} according to the reliability block diagram, and system-level B_{10} lifetime L_{B10_sys} can be seen from its unreliability curve. As shown in Fig. 9, the reliability evaluation flowchart is presented from the mission profile to component-level and system-level capacitor lifetime.

The key parameters related to the lifetime calculation are listed in Table 2. With the annual wind speed (Class I) and ambient temperature with a sample rate of 1 hour, the loss profile, thermal profile and the accumulated damage are shown in Fig. 10(a), (b), (c), respectively. In the case that the degrading ESR is considered, it can be seen that the loss dissipation and core temperature increase much more than in the case without the degradation. According to (2), as the core temperature of the capacitor is closely related to the ambient temperature, it can be seen that the annual core temperature profile is quite similar to the ambient temperature profile. Moreover, the core temperature is annually repeated due to the assumption of the same ambient temperature at different years. Furthermore, it is evident that the capacitor core temperature reaches the maximum operation temperature of 75 °C much earlier if the

degradation is taken into account. For the damage accumulation, it becomes exponential compared to linear increase without the degradation. Since the end-of-life of the capacitor is defined when the accumulated damage reaches 1, the increasing ESR in the degradation process significantly shorten the lifetime of capacitor. In the case of the zoom-in of the first year, it can be seen that the power loss, core temperature, and accumulated damage with or without degradation only differ slightly.

The stress profile of the capacitor along the operation period can also be investigated with different supply modes of the reactive power, as shown in Fig. 11. It can be seen that the UE injection relieves the stress compared to the NOR mode, while the OE injection increases the capacitor stress. The B_{10} lifetime of the individual capacitor can be found once the accumulated damage reaches 1.

As the B_{10} lifetime of the individual capacitor only indicates 10% probability of capacitor failure when the operation period reaches the predicted lifetime, without the component-level time-dependent reliability curve, it becomes difficult to link between the capacitor cell and capacitor bank. Since the same failure mechanism has an identical failure data distribution, the shape parameter of the Weibull distribution can be assumed at 5.13 [27], [28]. As a result, the B_{10} lifetime of each capacitor $L_{B10\_com\_i}$ can be extrapolated to time-to-failure curve F_{com_i} as indicated in Fig. 9.

As shown in Fig. 12(a), as any failure of the individual capacitor may result in the unreliable operation of the capacitor bank, all of the capacitors are connected in series in the reliability block diagram [27]. Under normal operation, the unreliability curve from the single capacitor to the capacitor bank is shown in Fig. 12(b). It can be seen that the 22 years B_{10} lifetime of the capacitor bank is significantly reduced due to a
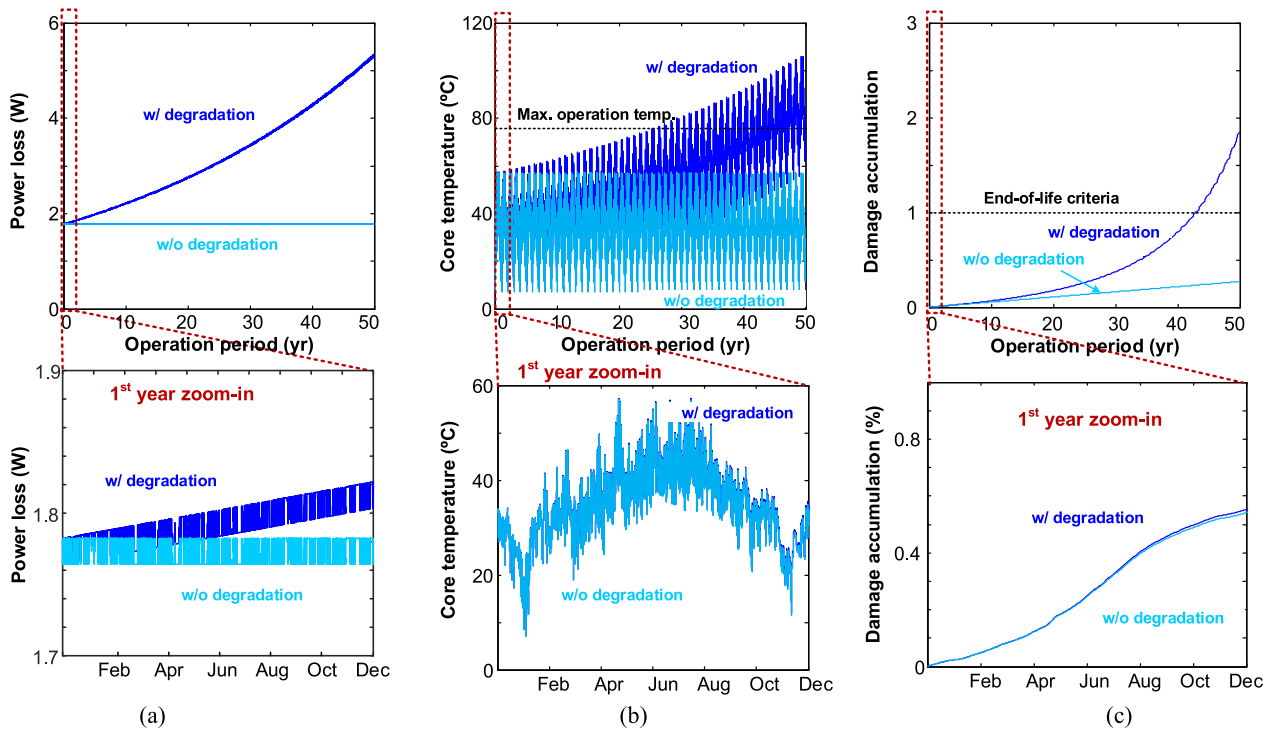
FIGURE 10. Profile comparison whether the degradation impact of capacitors are taken into account. (a) Power loss profile. (b) Thermal stress profile. (c) Accumulated damage.
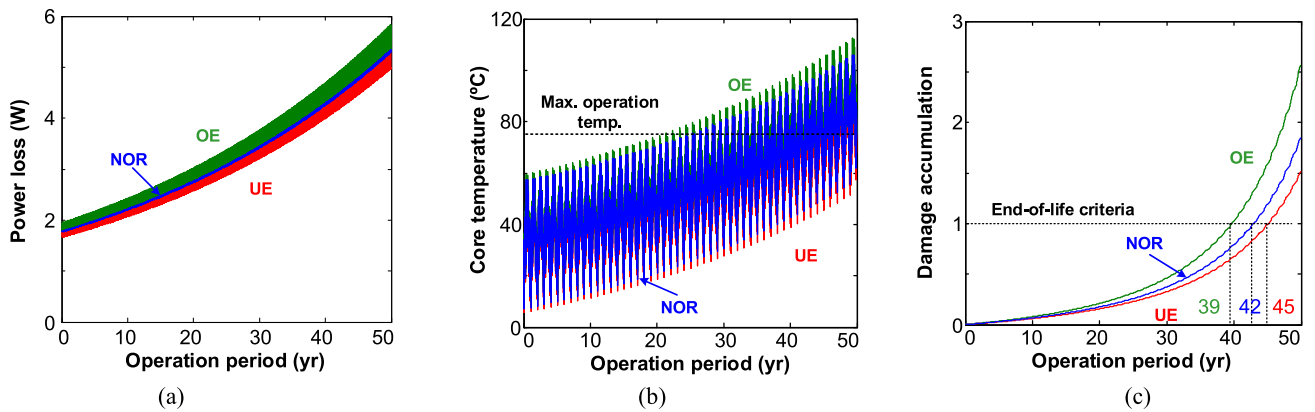

FIGURE 11. Profile comparison at various reactive power operation modes. (a) Power loss profile. (b) Thermal stress profile. (c) Accumulated damage. NOR denotes without reactive injection; UE denotes under-excited reactive power injection; OE denotes the over-excited reactive power injection.

large amount of applied capacitors, where the individual filter capacitor lifetime is with 42 years. Moreover, if the degrading ESR is not taken into account, it results in an over-estimated lifetime of the capacitor bank with 93 years. The reactive power impacts on system-level reliability of the capacitor bank is shown in Fig. 12(c). It is noted that, compared with the capacitor bank lifetime of 22 years at the normal operation, the OE reactive power reduces to 20 years, while the UE reactive power increases to 23 years due to various electrical stresses. With respect to the accumulated percentage of failure at the desired lifespan of 20 years, the value is 6.7% in the case

of the normal operation. However, the values become 4.8% and 10.0% under the UE and OE reactive power injection. Regardless of the operational models, the accumulated failure is below 10% at the desired 20-year lifespan, which indicates that the existing design of the filter capacitor bank is able to fulfill the lifespan requirement caused by thermal related wear-out.

V. CONCLUSION
Aiming for the grid-connected inverter of the wind power generation, a reliability analysis method of the LCL filter
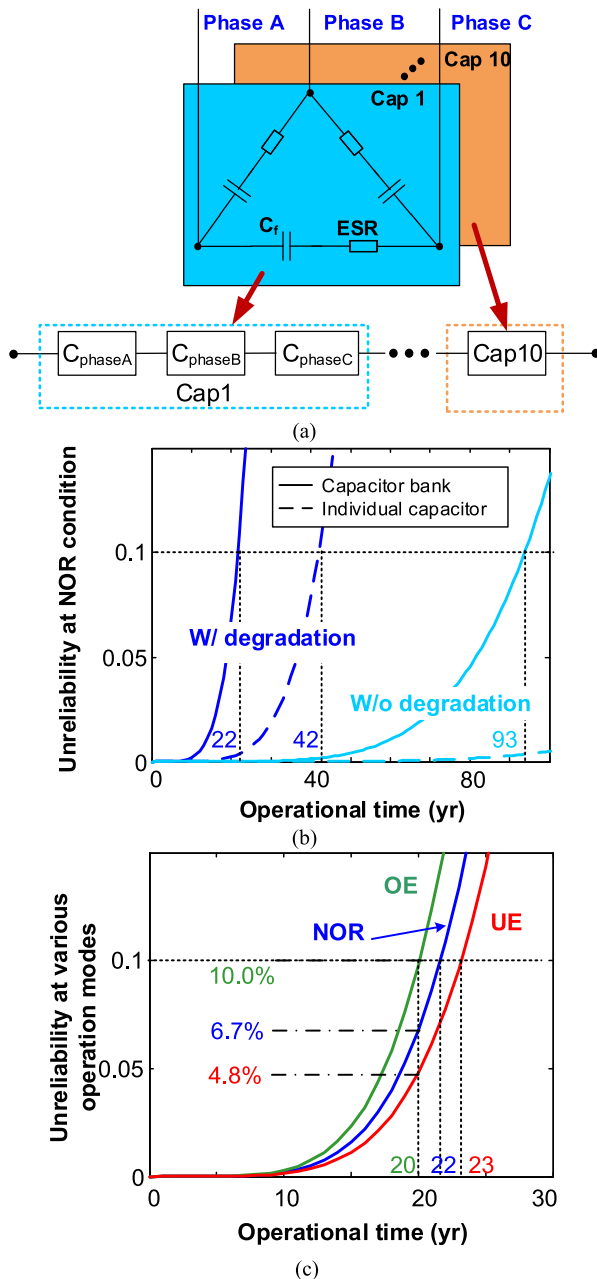
FIGURE 12. System-level reliability of capacitor bank. (a) Capacitor bank structure and reliability block diagram. (b) Unreliability curve from capacitor cell to capacitor bank at normal condition. (c) Capacitor bank reliability at normal (NOR), over-excited (OE), and under-excited (UE) reactive power injection.

capacitor, which is caused by thermal related wear-out, is described in this paper. Based on the electrical stresses of the filter capacitor at different reactive power requirements, the percentile lifetime of the single capacitor can be predicted according to annual thermal profile. The Weibull function based time-to-failure distribution of the single capacitor can further be converted into the filter capacitor bank reliability by using the reliability block diagram. A system-level reliability study of 2 MW wind turbine system is analyzed and compared

considering the degradation performance. It can be seen that the lifetime is significantly over-estimated by the ignorance of the parameter shifting of the ESR due to degradation. Moreover, assuming that the reactive power is supplied all year around, the over-excited reactive power injection reduces the lifetime compared to no reactive power injection, while the under-excited reactive power slightly prolongs the lifetime.

It is worthwhile to mention that only the thermal stress caused fatigue is the focus of this paper, which considers the ambient temperature and temperature increase caused by internal power loss of capacitor. The lifetime estimation becomes more accurate if other environmental conditions (e.g., contamination, humidity) and excessive thermal conditions (e.g., thermal cycling during real-world operation) are taken into account. In addition, the capacitors that went through accelerated lifetime testing are electrolytic capacitors, and the capacitors used in the 2 MW DFIG system are film capacitors. These are two different capacitor material and might have quite different failure mechanism, which might lead to different shape factor and scale factor. Compared with the filter capacitor used in the design, although the tested capacitors are not with same material, the general procedure to obtain the lifetime model of the capacitor is the same. The engineering insight offered by this paper is an algorithm to predict filter capacitor lifetime pending some reliable components and system parameters. While the selected Weibull distribution is obtained through experimental testing, the combination of stress analysis and strength modeling needs further experimental verification.

REFERENCES

[1] F. Blaabjerg and K. Ma, "Future on power electronics for wind turbine systems," *IEEE J. Emerg. Sel. Topics Power Electron.*, vol. 1, no. 3, pp. 139–152, Sep. 2013.

[2] A. Reznik, M. Simoes, A. Al-Durra, and S. Muyeen, "LCL filter design and performance analysis for grid-interconnected systems," *IEEE Trans. Ind. Appl.*, vol. 50, no. 2, pp. 1225–1232, Mar. 2014.

[3] Q. Wang, M. Cheng, Y. Jiang, W. Zuo, and G. Buja, "A simple active and reactive power control for applications of single-phase electric springs," *IEEE Trans. Ind. Electron.*, vol. 65, no. 8, pp. 6291–6300, Aug. 2018.

[4] B. C. Rabelo, W. Hofmann, J. L. da Silva, R. G. de Oliveira, and S. R. Silva, "Reactive power control design in doubly fed induction generators for wind turbines," *IEEE Trans. Ind. Electron.*, vol. 56, no. 10, pp. 4154–4162, Oct. 2009.

[5] S. Engelhardt, I. Erlich, C. Feltes, J. Kretschmann, and F. Shewarega, "Reactive power capability of wind turbines based on doubly fed induction generators," *IEEE Trans. Energy Convers.* vol. 26, no. 1, pp. 364–372, Mar. 2011.

[6] B. Sun, X. Fan, C. Qian, and G. Zhang, "PoF-simulation-assisted reliability prediction for electrolytic capacitor in LED drivers," *IEEE Trans. Ind.Electron.*, vol. 63, no. 11, pp. 6726–6735, Nov. 2016.

[7] K. Abdennadher, P. Venet, G. Rojat, J. M. Retif, and C. Rosset, "A realtime predictive-maintenance system of aluminum electrolytic capacitors used in uninterrupted power supplies," *IEEE Trans. Ind. Appl.*, vol. 46, no. 4, pp. 1644–1652, Jul. 2010.

[8] A. Lahyani, P. Venet, G. Grellet, and P. J. Viverge, "Failure prediction of electrolytic capacitors during operation of a switch-mode power supply," *IEEE Trans. Power Electron.*, vol. 13, no. 6, pp. 1199–1207, Nov. 1998.

[9] M. L. Gasperi, "Life prediction modeling of bus capacitors in ac variable frequency drives," *IEEE Trans. Ind. Appl.*, vol. 41, no. 6, pp. 1430–1435, Nov. 2005.

[10] X. Wang, M. Karami, and R. Tallam, "Test fixtures to apply variable DC bias and AC ripple current for reliability testing of electrolytic capacitors," *IEEE Trans. Ind. Appl.*, vol. 55, no. 4, pp. 4073–4079, Jul.-Aug. 2019.

[11] H. Wang *et al.*, "Transitioning to physics-of-failure as a reliability driver in power electronics," *IEEE J. Emerg. Sel. Topics Power Electron.*, vol. 2, no. 1, pp. 97–114, Mar. 2014.

[12] "Life cycle assessment of electricity production from an onshore V100-2.0 MW wind plant," Vestas Report, 2015.

[13] K. Ma, H. Wang, and F. Blaabjerg, "New approaches to reliability assessment: using physics-of-failure for prediction and design in power electronics systems," *IEEE Power Electron. Mag.*, vol. 3, no. 4, pp. 28–41, Dec. 2016.

[14] H. Oh, B. Han, P. McCluskey, C. Han, and B. D. Youn, "Physics-of-failure, condition monitoring, and prognostics of insulated gate bipolar transistor modules: A review," *IEEE Trans. Power Electron.*, vol. 30, no. 5, pp. 2413–2426, May. 2015.

[15] D. Zhou, H. Wang, and F. Blaabjerg, "Reactive power impacts on LCL filter capacitor lifetime and reliability in DFIG grid-connected inverter," in *Proc. IEEE Energy Convers. Congr. Expo.*, 2018, pp. 4094–4101.

[16] D. Zhou, G. Zhang, and F. Blaabjerg, "Optimal selection of power converter in DFIG wind turbine with enhanced system-level reliability," *IEEE Trans. Ind. Appl.*, vol. 54, no. 4, pp. 3637–3644, Jul. 2018.

[17] L. Malesani, L. Rossetto, P. Tenti, and P. Tomasin, "AC/DC/AC PWM converter with reduced energy storage in the DC link," *IEEE Trans. Ind. Appl.*, vol. 31, no. 2, pp. 287–292, Mar. 1995.

[18] E. ON-Netz. Requirements for offshore grid connections, Apr. 2008.

[19] M. Liserre, R. Cardenas, M. Molinas, and J. Rodriguez, "Overview of multi-MW wind turbines and wind parks," *IEEE Trans. Ind. Electron.*, vol. 58, no. 4, pp. 1081–1095, Apr. 2011.

[20] Recommended Practice and Requirements for Harmonic Control in Electric Power Systems, IEEE Stdandard 519, 2014.

[21] Jianghai Application Notes, "*Electrolytic capacitor lifetime estimation*," 2010. [Online]. Available: jianghai-america.com/uploads/technology/JIANGHAI_Elcap_Lifetime_-_Estimation_AAL.pdf

[22] V. H. Prasad, "Analysis and comparison of space vector modulation schemes for three-leg and four-leg voltage source inverters," Master dissertation, Virginia Tech, Blacksburg, USA, 1997.

[23] D. Zhou, F. Blaabjerg, T. Franke, M. Tønnes, and M. Lau, "Comparison of wind power converter reliability with low-speed and medium-speed permanent-magnet synchronous generators," *IEEE Trans. Ind.Electron.*, vol. 62, no. 10, pp. 6575–6584, Oct. 2015.

[24] Datasheet of Panasonic Aluminum Electrolytic Capacitors, 2019. [Online]. Available: https://industrial.panasonic.com/cdbs/www-data/pdf/RDF0000/ABA0000C1209.pdf

[25] "Aluminum Can Power Film Capacitors for PFC and AC Filter," KEMET datasheet, 2007

[26] Capacitor Lifetime Calculator, 2018. [Online]. Available: http://www.illinoiscapacitor.com/tech-center/life-calculators.aspx

[27] P. D. T. O'Connor and A. Kleyner, *Practical Reliability Engineering*. New York, NY, USA: Wiley2012.

[28] D. Zhou, Y. Song, Y. Liu, and F. Blaabjerg, "Mission profile based reliability evaluation of capacitor banks in wind power converters," *IEEE Trans. Power Electron.*, vol. 34, no. 5, pp. 4665–4677, May 2019.